Sensors and Actuators A 159 (2010) 24–32

Contents lists available at ScienceDirect

Sensors and Actuators A: Physical

journal homepage: www.elsevier.com/locate/sna

Electromagnetic fields distribution in multilayer thin film structures and the origin of sensitivity enhancement in surface plasmon resonance sensors

Atef Shalabney, Ibrahim Abdulhalim*

Department of Electro-Optic Engineering, Ben Gurion University, Beer Sheva 84105, Israel

ARTICLE INFO

Article history:
Received 6 October 2009
Received in revised form 8 January 2010
Accepted 7 February 2010
Available online 13 February 2010

Keywords:
Surface plasmon resonance
Optical sensors
Surface waves

ABSTRACT

The performance of surface plasmon resonance (SPR) sensors depends on the design parameters. An algorithm for calculating the electromagnetic fields distribution in multilayer structure is developed relying on Abeles matrices method for wave propagation in isotropic stratified media. The correlation between field enhancement and sensitivity enhancement is examined and found to agree with the overlap integral in the analyte region. This correlation was verified in the conventional SPR sensor based on Kretschmann configuration, and in the improved SPR sensor with high refractive index dielectric top layer for several cases, e.g. field enhancement due to resonance, the sensitivity dependence on the wavelength, the influence of prism refractive index on sensitivity, and the effect of the layers materials and thicknesses.

1. Introduction

Surface plasmon resonance (SPR) sensors are widely recognized as valuable tools for investigating surface interactions and sensing of gases and biomaterials [1]. A surface plasmon wave is a longitudinal compressional charge density wave that can propagate at the interface between a metal and a dielectric media under certain conditions. One of the most common techniques for plasmon excitation is the Kretschmann configuration shown in Fig. 1(a) in which the resonance realized by a dip in the reflectivity versus incidence angle or alternatively in the reflectivity versus wavelength. Since the dip location depends on the substrate (analyte) features, one can measure tiny fluctuations in the refractive index of the analyte by tracking either the shift in the resonance angle or the shift in the resonance wavelength [2–4].

Due to the pioneering works of Kretschmann [5] and Otto [6], practical devices were proposed for chemical and biological sensors applications. Several parameters and features define the performance quality of SPR sensor: (1) reflectance profile shape (dip depth and width), (2) chemical stability of the metal layer, (3) sensor resolution, and (4) sensor sensitivity. The sensor's sensitivity is defined as the ratio between the resonance angle or wavelength shift per analyte refractive index unit. Gent et al. [7] defined the sensitivity as the ratio between the shift and width of the dip. This definition is somehow misleading and questionable because several algorithms can be applied to determine the dip position with high accuracy even with moderate resolution. The later definition was considered by Golosovsky et al. [8] recently. They demonstrated that the sensitivity of SPR technique in the infrared range using Fourier transform infrared (FTIR) spectrometry is not lower compared to the sensitivity of the SPR technique in the visible range. In the present work we define the sensitivity as the dip shift per sample refractive index unit and will ignore dip width aspect in the sensitivity definition.

In the last two decades few methods were proposed to improve the SPR sensor sensitivity. Using long range SPR (LRSPR) sensor [9,10] where the excitation of two SP waves on the interfaces of the metal layer placed between two dielectric layers increases the propagation distance on the surfaces and correspondingly increases the sensitivity. Although many works reported sensitivity enhancement by measuring phase instead of intensity [11–14], recent study [15] showed that these reports are questionable and the accuracy in phase measurements is limited by the accuracy of intensity measurements. Another method to enhance SPR sensor sensitivity was using periodic metallic structures combined with TIR Kretschmann configuration [16,17]. Also the use of bimetallic layers [18–20], and modification of prism refractive index [21,22] were proposed in order to enhance SPR sensor sensitivity. Lahav et al. presented for the first time the nearly guided wave SPR (NGWSPR) configuration that is similar to the conventional configuration with the addition of 10–15 nm dielectric layer with a high refractive index between the metal layer and the cover material (the analyte to be sensed) [23,24] as shown in Fig. 1(b). The

* Corresponding author at: Ben Gurion University, Department of Electro-optic Engineering, P.O. Box 653, 84105 Beer Sheva, Israel. Tel.: +972 8 6479803.
E-mail addresses: shalaban@bgu.ac.il (A. Shalabney), abdulhlm@bgu.ac.il (I. Abdulhalim).

0924-4247/$ – see front matter © 2010 Elsevier B.V. All rights reserved.
doi:10.1016/j.sna.2010.02.005

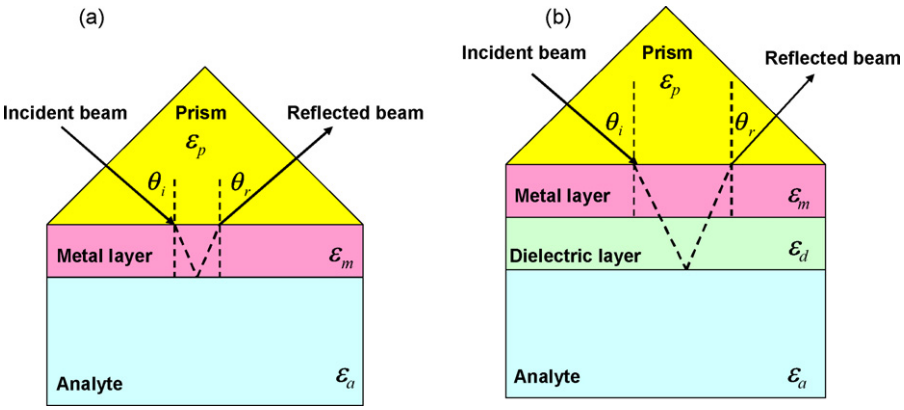

Fig. 1. (a) Schematic of single layer Kretschmann configuration and (b) schematic of double layer Kretschmann configuration.

authors choose silicon (Si) to accomplish the task because Si has high real part of refractive index. Lahav et al. configuration has two prominent advantages: first the sensitivity was enhanced by few times compared to conventional SPR sensor, and second the stability of the metal layer was improved because the silicon served as protection layer for the silver which suffers from a poor chemical stability. When the addition of a thin dielectric layer with a high refractive index on top of the metal layer is considered, one should emphasize that the added layer is very thin (typically 10 nm). One should distinguish this case from the case of coupled plasmon-waveguide resonance (CPWR). CPWR biosensors incorporate a thick waveguide layer (typically 500 nm) beneath the surface of the conventional SPR biosensor [25,26]. Unlike the conventional SPR biosensors, whose reflectivity demonstrates a dip only in the TM mode, the interference in the waveguide layer causes a dip both in the TE and TM modes in the CPWR device [27]. Although CPWR sensors exhibit sharp dips and improve significantly the SNR of the measurement, their sensitivity is less than that of conventional SPR devices by an order of magnitude since the biosensing surface is located at a considerable distance from the SPs which exist on the interface between the metal and the waveguide layer [28,29]. The contribution of a thin dielectric top layer to the sensitivity enhancement of SPR sensor was reported for the first time by Lahav et al. Because the nm-thick layer does not support guided modes, it was called nearly guided wave SPR (NGWSPR) sensor.

In the present work we investigate the sensitivity enhancement mechanism of SPR sensors by electromagnetic field and energy distribution considerations. Since the SPR is accompanied by an enhanced evanescent field in the metal–analyte interface region, the sensor sensitivity for a perturbation in the analyte is determined by the field distribution in this region. According to Abdulhalim [30], the shift in the wave vector is proportional to the overlap integral which in turn is proportional to the interaction volume V_{in} (see Appendix A):

$$\delta k \approx \frac{k_i}{2} \frac{\int_{V_{in}} \delta\varepsilon \cdot \vec{E}_i^* \cdot \vec{E}_f \cdot dr}{\int_V \varepsilon \cdot \vec{E}_i^* \cdot \vec{E}_i \cdot dr} \quad (1)$$

where E_i, k_i are the electrical field and its wave vector before the variation in the analyte refractive index took place, while E_f is the field after the index perturbation and δk is the associated shift in the wave vector due to a change from ε to $\varepsilon+\delta\varepsilon$ in the analyte dielectric constant. Since δk expresses the change in the incidence angle or alternatively the change in the wavelength, then $\delta k/\delta\varepsilon$ represents the sensitivity of the sensor, which is proportional to the overlap integral in the numerator of Eq. (1) normalized to the total energy. Hence to maximize the sensitivity one needs to maximize this integral which can be accomplished by increasing the interaction volume, that is the evanescence depth, the SP propagation length along the surface or by increasing the field intensity in the analyte region. One of our purposes in this paper is to demonstrate that sensitivity enhancement mechanisms are accompanied with field enhancement and correlated with the overlap integral in the analyte region.

Full description of the electromagnetic field in multilayer structures within the SPR modes context was done by Davis [31] where the purpose was obtaining the eigenfunctions of the differential equation for the magnetic field distribution and simultaneously the eigenvalues were derived from the dispersion relation. Chin et al. [32] presented calculations for electromagnetic field distribution by matrices approach to extract the reflectivity for the multilayer structure. In both previous works [31,32], they used propagation matrices to calculate the two components of the forward and backward propagating magnetic field amplitudes in arbitrary layer from the boundary values of the aforementioned amplitudes. Ohta et al. [33] proposed a method to calculate the forward and backward propagating electric field without using inverse matrices; however, he described the full fields by exponential expressions which may be problematic due to some numerical instability. Ekgasit et al. [34] and Hansen [35] used the characteristic matrices approach and the total transmission coefficients for explaining their SPR spectroscopy experiments; however, they only emphasized absorbance aspects in multilayer system. The uniqueness of our work is in that it involves a detailed simplified algorithm for electromagnetic field distribution and full comprehensive investigation for the evanescent field role in sensitivity enhancement which was never done before to the best of our knowledge.

2. The algorithm for field distribution

We consider the general case of plane wave radiation interacting with a stack of $N-1$ layers as shown in Fig. 2 so that we have N interfaces. The layers are homogenous and isotropic with plane boundaries, the optical properties of each layer are characterized completely by two constants which are functions of wavelength, e.g. the dielectric constant $\varepsilon_j = n_j^2$ where n_j the refractive index for layer-j and the magnetic permeability is μ_j. The constants ε_j, n_j, μ_j are complex in the general case. Under the SPR conditions, the electric field must have a component which is perpendicular to the surface; hence the incident light should be TM polarized. We take the plane of incidence to be the XZ-plane and the Z-axis is the direction of stratification. For TM wave, $H_x = H_z = 0$ and $E_y = 0$. The non-vanishing components of the field vectors into each layer-j are

of the form:

$$H_{yj}(x,z,t) = H_{yj}(z)\ \exp\left\{i(k_0\alpha_j x - \omega t)\right\},$$
$$E_{xj}(x,z,t) = E_{xj}(z)\ \exp\left\{i(k_0\alpha_j x - \omega t)\right\}, \quad (2)$$
$$E_{zj}(x,z,t) = E_{zj}(z)\ \exp\left\{i(k_0\alpha_j x - \omega t)\right\},$$

here $H_{yj}(z)$, $E_{xj}(z)$, $E_{zj}(z)$ are the amplitudes of the appropriate fields in layer-j that are in general complex functions of z; $\alpha_j = n_j \sin\theta_j$ when θ_j the propagation angle and $k_0 = 2\pi/\lambda_0$ the wave number in vacuum. According to Snell's law one can consider the following:

$$\alpha_j = n_j\ \sin\theta_j = \text{const} = \alpha = n_0 \sin\theta_0 \quad (3)$$

When the general structure shown in Fig. 2 constitutes an SPR sensor, the substrate and the ambient will represent the analyte and the prism, respectively, to be consistent with Fig. 1. As was mentioned in the introduction, methods for calculating field's distribution in N layered structure were presented by several investigators [33–35], however, as algorithms we found them not clear enough and difficult to use particularly for researchers from the biosciences and bio-technology. In the present section we introduce a detailed and simplified algorithm for field distribution calculation. Our description completely detailed to allow convenience numerical implementation in three steps.

Step 1: Calculating total characteristic matrix, reflection and transmission coefficients for the whole structure. The magnetic and electric fields amplitudes in the entrance of each layer are connected to the corresponding amplitudes at a distance z inside the layer by the well known Abeles [36] matrices:

$$\begin{bmatrix} H^0_{yj} \\ -E^0_{xj} \end{bmatrix} = M_j \cdot \begin{bmatrix} H_{yj}(z) \\ -E_{xj}(z) \end{bmatrix} = \begin{bmatrix} \cos\beta_j & -\dfrac{i}{q_j}\sin\beta_j \\ -iq_j \sin\beta_j & \cos\beta_j \end{bmatrix} \cdot \begin{bmatrix} H_{yj}(z) \\ -E_{xj}(z) \end{bmatrix} \quad (4)$$

H^0_{yj}, E^0_{xj} are the amplitudes of H_{yj}, E_{xj}, respectively, at the appropriate boundary $z = Z_j$ of layer-j, M_j is called the characteristic matrix for the layer-j and it is determined by the optical properties and the layer thickness (d_j) where: $\beta_j = k_0 n_j d_j \cos\theta_j$; $q_j = \sqrt{(\mu_j/\varepsilon_j)}\cos\theta_j$.

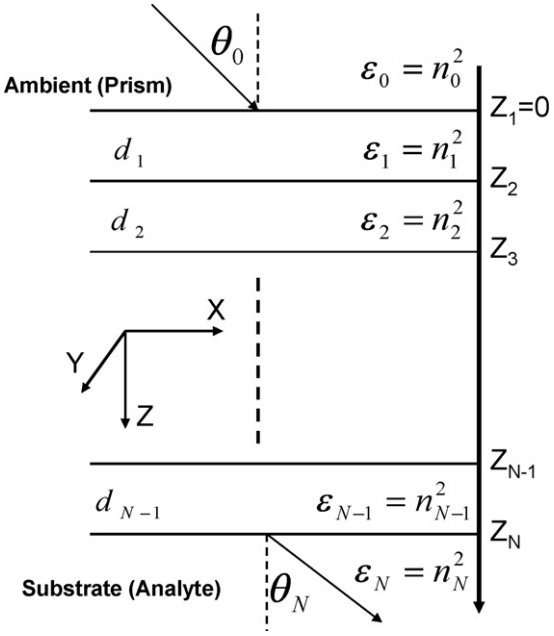

Fig. 2. Interaction of plane wave with a multilayer system, the stack composed of $(N-1)$ homogenous and isotropic media with N interfaces that bounded by two semi-infinite homogenous, isotropic, and dielectric media.

For a multilayered structure the field amplitudes at the first boundary are connected to those at the last boundary by the total characteristic matrix:

$$\begin{bmatrix} H^0_{y1} \\ -E^0_{x1} \end{bmatrix} = M_{\text{TOT}} \cdot \begin{bmatrix} H^0_{yN} \\ -E^0_{xN} \end{bmatrix}, \qquad M_{\text{TOT}} = \prod_{j=1}^{j=N-1} M_j \quad (5)$$

The complex reflection and transmission coefficients r and t can be expressed in terms of the elements of the total characteristic matrix of the whole system M_{ij}:

$$r \equiv \frac{H^{ref}_y}{H^{inc}_y} = \frac{(M_{11} + M_{12}\cdot q_N)\cdot q_0 - (M_{21} + M_{22}\cdot q_N)}{(M_{11} + M_{12}\cdot q_N)\cdot q_0 + (M_{21} + M_{22}\cdot q_N)}$$
$$t \equiv \frac{H^0_{yN}}{H^{inc}_y} = \frac{2\cdot q_0}{(M_{11} + M_{12}\cdot q_N)\cdot q_0 + (M_{21} + M_{22}\cdot q_N)} \quad (6)$$

H^{inc}_y, H^{ref}_y are the incident and reflected magnetic field amplitudes, H^0_{yN} is the transmitted magnetic field amplitude and simultaneously the amplitude at the last interface ($z = Z_N$).

Step 2: Calculating the field within the 1st layer:

$$\begin{bmatrix} H_{y1}(z) \\ -E_{x1}(z) \end{bmatrix} = P_1(z) \cdot \begin{bmatrix} (1+r) \\ q_0(1-r) \end{bmatrix} H^{inc}_y, \quad Z_1 \le z \le Z_2 \quad (7)$$

where $P_1(z)$ is given by:

$$P_1(z) = \begin{bmatrix} \cos(k_0 n_1 z\cos\theta_1) & \dfrac{i}{q_1}\sin(k_0 n_1 z\cos\theta_1) \\ iq_1 \sin(k_0 n_1 z\cos\theta_1) & \cos(k_0 n_1 z\cos\theta_1) \end{bmatrix} \quad (8)$$

And the incident magnetic field amplitude maybe taken as unity: $H^{inc}_y = 1$ for normalized magnetic field, while if one needs to normalize the electric field to the incident electric field amplitude, the following substitution $H^{inc}_y = E^{inc}_x/q_0$ should be used in equations (7) and (9).

Step 3: Calculating the field distribution within layer-$j \ge 2$ from the following expression:

$$\begin{bmatrix} H_{yj}(z) \\ -E_{xj}(z) \end{bmatrix} = P_j(z) \cdot \left(\prod_{l=j-1}^{1} P_l(z = Z_l + d_l) \right) \cdot \begin{bmatrix} (1+r) \\ q_0(1-r) \end{bmatrix} H^{inc}_y,$$
$$Z_j \le z \le Z_{j+1} \quad (9)$$

where $P_j(z)$ is the propagation matrix for the layer-j (inverse of the characteristic matrix $M_j(z)$) and it is given by:

$$P_j(z) = \begin{bmatrix} \cos(k_0 n_j (z - Z_j)\cos\theta_j) & \dfrac{i}{q_j}\sin(k_0 n_j (z - Z_j)\cos\theta_j) \\ iq_j \sin(k_0 n_j (z - Z_j)\cos\theta_j) & \cos(k_0 n_j (z - Z_j)\cos\theta_j) \end{bmatrix} \quad (10)$$

One should be careful when distinguishing between $P_j(z)$ and $P_l(z = Z_l + d_l)$ that appear in Eq. (9). While the first is z-dependent as was defined through Eq. (10), the second is the propagation matrix for the layer-l with thickness d_l, which is constant for layer-l. Normalizing to the incidence magnetic field amplitude could be achieved by setting H^{inc}_y to unity. Since in many cases the SPR sensor structure is composed of a single metal layer which is embedded between two semi-infinite dielectric media, namely, the prism and the analyte, the distribution expression in this case was separated and represented by step 2.

For TE polarization all the expressions for the characteristic and propagation matrices and reflection or transmission coefficients are valid simply by replacing the expression for $q_j = \sqrt{(\mu_j/\varepsilon_j)}\cos\theta_j$ with $p_j = \sqrt{(\varepsilon_j/\mu_j)}\cos\theta_j$ and the field column for TE is $\begin{bmatrix} E_{yj} \\ H_{xj} \end{bmatrix}$.

3. Applications

Our 2nd purpose in this work is to investigate the origin of sensitivity enhancement in SPR sensors based on Kretschmann configuration. From Eq. (1) the sensitivity proportional to the ratio between the energy flow in the analyte region and the total energy. In this sense we intend to examine the correlation between sensitivity enhancement and the field's distribution for several cases. In part of the cases, we deal with the conventional configuration as shown in Fig. 1(a), and afterwards with the improved configuration as shown in Fig. 1(b).

In the simulations the resonance angle was calculated with accuracy of $\Delta\theta = 0.001^\circ$ and the variation in the analyte refractive index was $\Delta n_a = 0.01$ RIU. Hence the sensitivity accuracy obtained to be $\Delta S = 0.01^\circ$/RIU. For field calculations, the amplitudes were computed in steps of $\Delta z = 0.5$ nm.

3.1. Evanescent field treatment for the standard Kretschmann configuration

First we consider the basic configuration shown in Fig. 1(a). The surface plasmon wave at the metal/dielectric interface is excited if the wave vector in *X*-direction of the incident wave matches that of the surface plasmon. When the surface plasmon is excited, a substantial decrease in reflectance is observed at the resonance angle, θ_r as shown in Fig. 3(a). The resonance angle, θ_r depends on the analyte refractive index, $n_a = \sqrt{\varepsilon_a}$ so that a change in the refractive index causes an appropriate shift in the resonance angle, see Fig. 3(b). The ratio between the angle shift and the refractive index change is defined as the angular sensitivity S_θ ($S_\theta = d\theta_r/dn_a$).

At the resonance, the reflectivity *R* reaches its minimum value, the intensity of the electromagnetic field reaches its maximum at the surface, see Fig. 4. Near the resonance angle, an extremely strong evanescent field at the metal/dielectric interface is generated by the surface plasmon wave. The unique characteristic of generating evanescent filed, where the field amplitude is greatest at the interface and exponentially decaying as a function of distance from the metal/dielectric interface, makes the SPR signal very sensitive to changes at the vicinity of the metal surface.

The *X*-component of the electric field is continuous; however, the *Z*-component is discontinuous. Due to the small dielectric constant of the analyte (ε_a) compared to that of the metal ($|\varepsilon_m|$), $|E_z|$ has a strong enhancement at the metal/analyte interface. As shown in Fig. 4(a) and (b) the enhancement of the electric field is largest at the resonance compared to the cases near the resonance, where the resonance angle in this case is $\theta_{res} = 54.619^\circ$.

Since there is a need sometimes of detecting at various wavelengths, sensitivity versus wavelength investigation is essential. As shown in Fig. 5(a), the sensitivity of the configuration described in Fig. 1(a) decreases when the wavelength increases. This result was presented by Homola [37] for the Kretschmann configuration without physical interpretation. Now in terms of the evanescent field, we can attribute the high sensitivity for lower wavelength to the larger interaction of the electric field in the analyte region. Although for larger wavelengths there is a larger penetration depth into the analyte region, the amplitude becomes smaller, which indicates that sensitivity is not governed only by the penetration depth, see Fig. 5(b), rather by both the interaction region and the energy distribution as expressed by the overlap integral of Eq. (1).

The sensitivity versus wavelength was calculated after performing optimization of the metal layer thickness. The silver layer thickness was chosen such that the resonance condition is preserved for each examined wavelength and the reflectivity at the dip is less than 0.01. As seen from the caption of Fig. 5, the silver thickness is decreasing when increasing wavelength. The losses in the metal increases with wavelength, and in order to overcome these losses and preserve resonance condition, the thickness should be reduced. In this case the sensitivity is approximately constant for large wavelengths, because in the IR range the sensitivity is mainly governed by the difference between the prism refractive index and the analyte refractive index $S_\theta = (d\theta/dn_a) \underset{\lambda\to\infty}{\longrightarrow} (1/\sqrt{n_p^2 - n_a^2})$(rad/RIU).

3.2. Evanescent field treatment for SPR sensor with nm-thick top dielectric layer

As pointed our before, the addition of a thin dielectric layer with a high real part of the refractive index causes substantial enhancement in the sensor sensitivity. Silicon was chosen for its high real part of the refractive index because the sensitivity enhancement was found [23,24] to increase with the real part of the dielectric constant of the top layer. As an optimization process for the silicon layer thickness, $d_{Si} = 10.5$ nm is the optimum thickness for maximum sensitivity as shown in Fig. 6(a). The evanescent field distribution demonstrates that for this silicon layer thickness, maximum enhancement ratio for the amplitude E_x is obtained. The addition of the silicon layer increases the sensitivity by threefold, e.g. 67.5°/RIU sensitivity without the silicon layer, compared with 200°/RIU sensitivity with $d_{Si} = 10.5$ nm silicon top layer.

The optimum silicon thickness of $d_{Si} = 10.5$ nm was chosen for 43 nm silver layer thickness because it gave the highest sensitivity enhancement. As done before with the standard Kretschmann configuration, one can perform an optimization for the improved sensor with the silicon dielectric layer. The sensitivity dependence on the wavelength has been examined for the improved sensor, and the same proportion was obtained. As shown in Fig. 7(a) and (b), a similar behavior for the sensitivity versus wavelength is obtained,

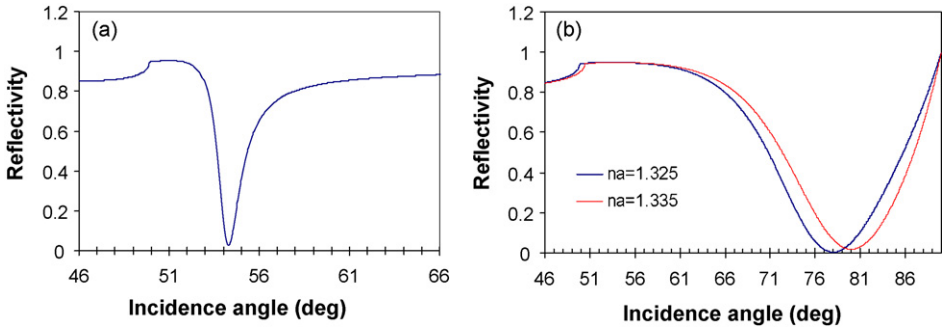

Fig. 3. (a) Reflectivity as a function of incidence angle for the configuration shown in Fig. 1(a). (b) Reflectivity versus analyte refractive index for the configuration shown in Fig. 1(b). $\lambda = 633$ nm, $d_m = 43$ nm, $n_p = 1.732$, $\theta_r = 54.61^\circ$, $n_a = 1.325$ (blue curve), $n_a = 1.335$ (red curve), silicon refractive index at 633 nm is $n_s = 3.8354 + 0.0245i$ and the silver refractive index is $n_s = 0.1325 + 4.0203i$. (For interpretation of the references to color in this figure legend, the reader is referred to the web version of the article.)

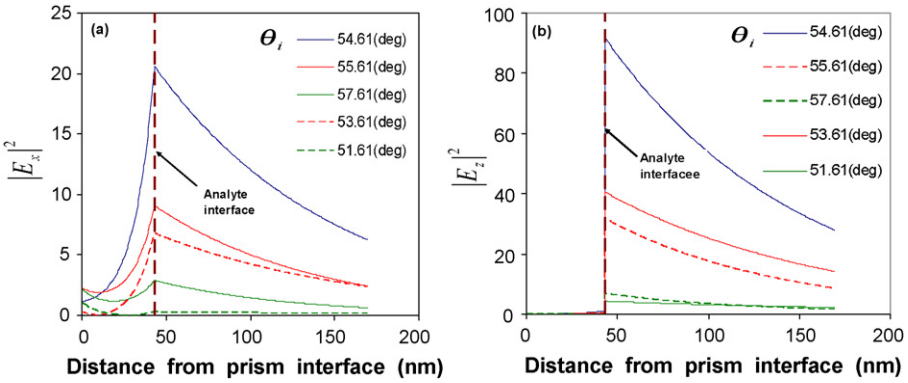

Fig. 4. (a) The density distribution of the *X*-component of the electric field. (b) The density distribution of the *Z*-component of the electric field through the layers at different incidence angles at and near the resonance. Both graphs correspond to the following parameters: $\lambda = 633$ nm, $d_m = 43$ nm, $n_a = 1.33$, $n_p = 1.732$, $\theta_r = 54.61^\circ$.

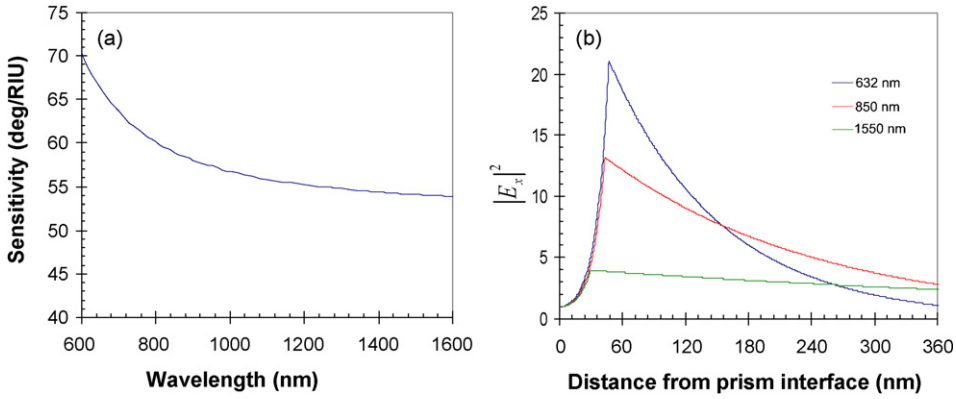

Fig. 5. (a) Sensitivity versus wavelength corresponding to the configuration in Fig. 1(a). (b) The density distribution of the electric field *X*-component along the metal and the analyte regions for different wavelengths at the resonance. $d_m = 43$ nm, $n_a = 1.33$, $n_p = 1.732$. The thicknesses for obtaining resonance in each wavelength are: 47, 43.25, and 29.75 nm for 632, 850, and 1550 nm, respectively.

except that in the case with the silicon layer the sensitivity starts from a higher value compared to the case without the silicon layer.

The origin of the sensitivity enhancement with decreasing the operation wavelength is basically related to the metal behavior. Both the real part and the imaginary part of the metal refractive index are responsible for the transparency features of the metal layer and they become larger when increasing the wavelength. Increasing the real part makes the metal more reflective from the initial prism/metal interface, whereas increasing the imaginary part makes it more absorptive and as a result of the double effect the evanescent field experiences more attenuation when it propagates through the whole system. When the refractive index of the metal changes from $0.12 + 3.75i$ at 600 nm wavelength up to $0.53 + 10.43i$ at 1500 nm, the amplitude of the fields at the analyte interface are significantly attenuated and consequently the sensitivity of the structure becomes moderate. Although the penetration depth was found to be 94 and 697 nm at 600 and 1500 nm wavelengths, respectively, in the conventional Kretschmann SPR sensor configuration, the sensitivity is still larger for smaller wavelength. The values were calculated from the following expression of the penetration depth:

$$\delta_d = \frac{\lambda}{4\pi}\sqrt{\frac{\varepsilon_a + \varepsilon_{mr}}{-\varepsilon_a^2}} \tag{13}$$

Here δ_d is the penetration depth inside the analyte layer, λ, ε_a, ε_{mr} are the wavelength, analyte dielectric constant, and the metal real part dielectric constant, respectively. This last fact indicates that

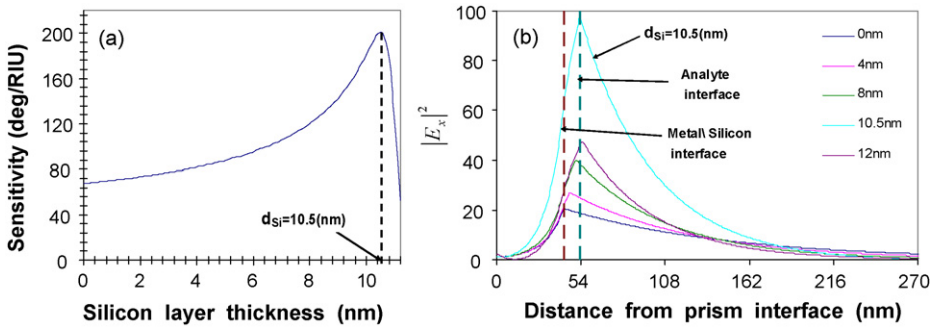

Fig. 6. (a) Sensitivity versus silicon layer thickness corresponding to the configuration in Fig. 1(b). (b) Density distribution of the electric field *X*-component for different Si layer thicknesses.

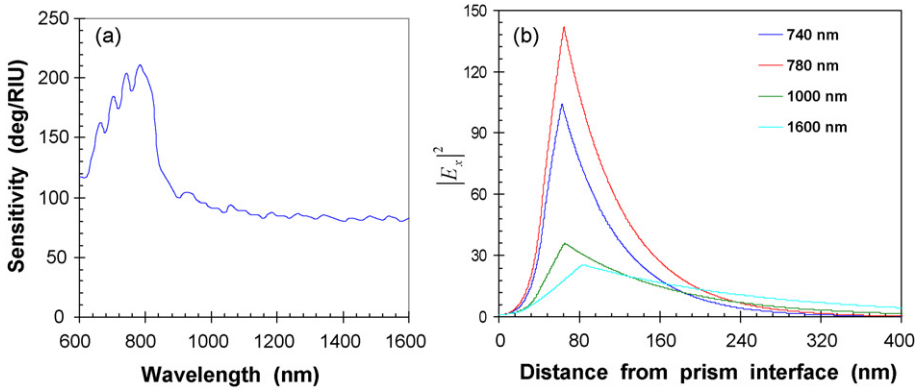

Fig. 7. (a) Sensitivity versus wavelength in the Kretschmann configuration with the silicon layer shown in Fig. 1(b). (b) The density distribution of the electric field X-component through the layers at different resonance wavelengths. The silicon refractive indices are: $3.64+0.0085i$; $3.59+0.0057i$; $3.4+0.0002i$; $3.22+0.002i$ at 740, 780, 1000 and 1600 nm, respectively, and ($n_a = 1.33$, $n_p = 1.732$). The silver and silicon thicknesses in this case were chosen under the resonance condition $R_{min} < 0.01$ for each wavelength. Table 1 shows the corresponding thicknesses and sensitivities for (b).

Table 1
Silver and silicon layers thicknesses that were chosen for each wavelength that appear in Fig. 7(b) in order to preserve $R_{min} < 0.01$ as a condition for resonance. The sensitivity and the E_x intensity at the analyte interface were calculated for each wavelength.

λ (nm) wavelength	d_m (nm) metal thickness	d_s (nm) silicon thickness	Sensitivity (°/RIU)	Field intensity at the analyte interface
740	45.5	17	204	103
780	44.5	20	210	141
1000	40	25	105	36
1600	29	54	82	25

sensitivity as it was defined in the present study is not governed only by the penetration depth. Absorption considerations will be further discussed in Eqs. (14) and (15) in Section 3.3. Sensitivity versus wavelength with the silicon top layer was calculated when the structure was optimized to fulfill the resonance condition at each wavelength. Table 1 shows the combinations (d_m, d_s) of the silver and the silicon thicknesses that maintain the structure at resonance, with reflectivity dip level of $R_{min} < 0.01$.

3.3. Sensitivity enhancement due to prism refractive index modification

The prism refractive index has an important role in the sensitivity determination of the SPR sensor based on TIR configuration. Two works [21,22] were recently published on this issue, and both showed that the sensitivity increases with decreasing the prism refractive index. The first work was on the sensitivity enhancement with the angular interrogation mode [21], in which the authors demonstrated the prism influence without giving any physical explanation for the phenomenon. In the second work which was done by Yulk et al. [22], the spectral interrogation mode was considered and the sensitivity enhancement was attributed to the large penetration depth obtained in the case of small prism refractive index. Under the last hypothesis, the sensitivity for a large wavelength should be larger than the sensitivity for smaller wavelength for all the cases, while we showed the opposite in the former discussion when we examined the wavelength influence on the sensitivity. Hence the explanation that was given by Yulk et al. is inadequate in our opinion. Our approach is based on the correlation between sensitivity and overlap integral in the analyte region. Larger enhancement for the electric field at the metal/dielectric interface for smaller prism refractive index was observed as shown in Fig. 8.

Fig. 8(a) and (b) clearly demonstrates the correlation between the sensitivity enhancement and the field enhancement. The case demonstrated by Fig. 8(a) and (b) relates to fixed operation wavelength (λ = 632 nm) while the variation is in the prism refractive index which in turn varies the incidence angle. The sensitivity versus prism refractive index was calculated when the metal layer thickness is optimized under the resonance condition ($R_{min} < 0.01$), where R_{min} is the dip level at resonance. Considering the Kretschmann configuration, the resonance condition obtained by equating the SP wave vector and the emerging light wave vector which can explicitly be written as $k_0 n_p \sin\theta = k_0\sqrt{(\varepsilon_{mr} n_a^2/(\varepsilon_{mr}+n_a^2))}$ where n_a and n_p are the analyte and the prism refractive indices, respectively, and ε_{mr} is the real part of the metal refractive index. By analyzing the last condition one can conclude that the coupling condition is fulfilled if $|\varepsilon_{mr}|$ is higher than the quantity $\eta = (n_a^2 \cdot n_p^2/(n_p^2 - n_a^2))$ which corresponds to having the resonance angles $\theta \leq 90°$. For a fixed wavelength, the last condition creates a singularity in the sensitivity for a prism refractive index which allows the quantity η to approach $|\varepsilon_{mr}|$ at the given wavelength. The last interpretation properly explains the dramatic increase in the sensitivity for $n_p \approx 1.41$ in Fig. 8(a) for a wavelength of 633 nm. In a similar manner the influence of the prism refractive index was investigated for the NGWSPR, and similar behavior of the sensitivity versus prism refractive index was found as the conventional SPR sensor. Results are shown in Fig. 9(a) and (b).

In the case of NGWSPR, there is a shift in the cut-off wavelength which can be clearly seen in the resonance angle positive shift due to the addition of the silicon layer. Basically, the incident light feels a higher refractive index beyond the metal layer and therefore, an appropriate modification in the dispersion relation of the SP. Since the wavelength is kept fixed, the resonance condition is satisfied at larger angle. The sensitivity in the NGWSPR case was calculated when the silver–silicon structure is optimized to maintain the resonance condition ($R_{min} < 0.01$); the values correspond to the field intensity distribution in Fig. 9(b) are given in Table 2.

Enhancing the fields at the metal interface increases the absorption as well as increasing the sensitivity of the structure. For conventional SPR sensor without dielectric layer, the only absorbing medium in the system is the metal film. When adding the silicon layer, the absorption will be both in the metal and the silicon layer. The absorption in the whole system can be expressed by the fol-

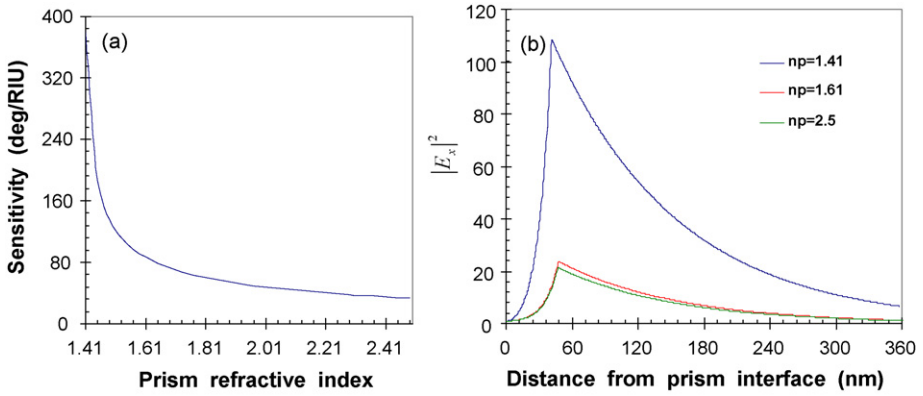

Fig. 8. (a) Sensitivity versus prism refractive index for the basic configuration shown in Fig. 1(a). (b) Density distribution for the electric field *X*-component through the layers for the same configuration given in Fig. 1(a) at different prism indices. The wavelength, silver layer thickness, and analyte refractive index are: $\lambda = 632$ nm, $d_m = 43$ nm, $n_a = 1.33$. The metal layer thicknesses that were chosen to obtain resonance for each prism refractive index are: 41.5, 47.5 and 47 nm for 1.41, 1.61, and 2.5 prism refractive index, respectively.

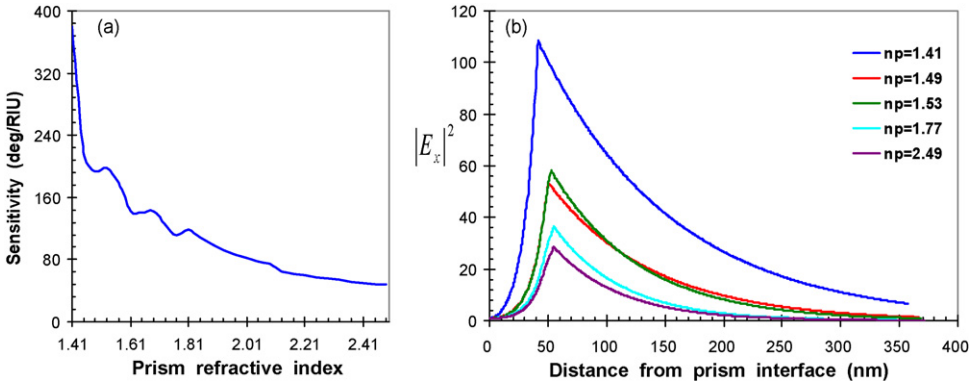

Fig. 9. (a) Sensitivity versus prism refractive index for the SPR sensor with silicon top layer given in Fig. 1(b). (b) Density distribution for the electric field *X*-component through the layers for the configuration given in Fig. 1(b) at different prism refractive indices. $n_a = 1.33$, $\lambda = 632$ nm. The silver and silicon thicknesses in this case were chosen under the resonance condition $R_{min} < 0.01$ for each prism refractive index. Table 2 shows the corresponding thicknesses and sensitivities for (b).

lowing approximation [34]:

$$A = \frac{2\pi}{\lambda} \cdot \frac{1}{k_{ZP}} \left\{ \int_0^{d_m} Im(\varepsilon_m) \cdot |E|^2 \cdot dz + \int_{d_m}^{d_m+d_s} Im(\varepsilon_s) \cdot |E|^2 \cdot dz \right\} \quad (14)$$

where here d_m, d_s are the metal and the silicon layers thicknesses, k_{ZP} the *Z*-component of the wave vector in the prism. Under the TIR, the transmittance T equals zero, and the reflectance can be expressed by the field's distribution according to: $R(\theta) = 1 - A(\theta)$. When the prism refractive index decreases, the dip becomes wider and the resonance is obtained at larger angles. Decreasing prism refractive index enhances the fields both in the metal and at the analyte interfaces, and the absorption in the metal becomes larger via the integral in Eq. (14) which causes widening to the dip nearby the resonance.

The overlap integral combines the enhanced amplitude in the analyte interface and the penetration depth into the analyte region, in such a way that the sensitivity may not be governed by only one of them. In order to verify the relation between the sensitivity and the overlap integral, we have calculated the integral of $|E_x|^2$ in the analyte region. Since the component of the electric field in the *X*-direction is a function of the vertical distance *z* into the analyte, the following integral was calculated which represents basically the overlap integral:

$$O \equiv \frac{1}{\lambda} \int_{z_1=Z_a}^{z_2=Z_a+\lambda} |E_x(z)|^2 \, dz \quad (15)$$

where z_1 and z_2 are the borders of the integral, and they are equal to Z_a and $Z_a + \lambda$, respectively, as shown in Fig. 1(b) where here Z_a is the silicon/analyte interface distance from the prism interface, and $Z_a + \lambda$ is placed at a one wavelength depth into the analyte region. The integral borders were determined in this way due to the fact that the electric field in the analyte region is evanescent, and after one wavelength distance it decays approximately to zero (Fig. 10).

Table 2
Silver and silicon layers thicknesses that were chosen for each prism refractive index that appears in Fig. 9(b) in order to preserve $R_{min} < 0.01$ as a condition for resonance. The sensitivity and the E_x intensity at the analyte interface are calculated for each wavelength.

n_p prism refractive index	d_m (nm) metal thickness	d_s (nm) silicon thickness	Sensitivity (°/RIU)	Field intensity at the analyte interface
1.41	41.5	0	380	108
1.49	47.5	3	193	53
1.53	47.5	5	197	58
1.77	47	8	111	36
2.49	47	8	48	28

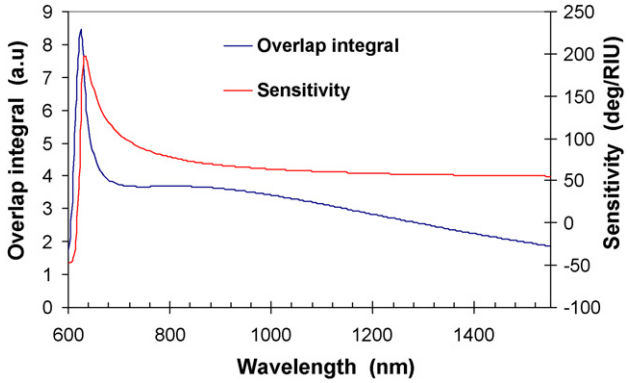

Fig. 10. The overlap integral for the electric field intensity in the *X*-direction and the sensitivity as a function of wavelength. Both the overlap integral, and the sensitivity were calculated using the parameters: $d_m = 43$ nm, $d_s = 10.5$ nm for the silver layer and the silicon layer thicknesses, respectively. $n_a = 1.33$, $n_p = 1.732051$ are the analyte refractive index and the prism refractive index, respectively.

Although the overlap integral was evaluated for a one case, the chosen case involves the silicon layer with the optimum thickness in addition to the silver layer. This structure is in the centre of our interest when we investigate the NGWSPR sensor. The maximum value for the overlap integral was obtained at a wavelength of 625 nm whereas the counterpart value for the sensitivity was obtained at 630 nm. Apart from this small difference, both the sensitivity and the overlap integral demonstrate the same behavior as a function of the wavelength. This small difference can be simply due to the fact that the sensitivity as described by the overlap integral in Eq. (1) is an approximate expression based on the 1st order perturbation theory [30].

4. Conclusions

The evanescent field produced at the analyte interface is the main characteristic of the surface plasmon resonance phenomenon as it is responsible for the sensing process that occurs at the analyte region. For the purpose of investigating the distribution of the field intensity within the layers in the SPR sensor, a practical and detailed numerical algorithm was developed. The algorithm may serve to understand the energy flow behavior as well as absorption and propagation of the surface plasmon waves generated at the metal surface. Such algorithm can be used for the case of long range SPR (LRSPR) configuration, which we plan to investigate in the future. The sensitivity of the SPR sensor in the Kretschmann configuration is governed by the ratio between the overlap integral in the analyte region, and the total energy of the propagating mode. The later expression constitutes a novel approach which provides an explicit physical interpretation for the SPR sensitivity concept. Based on this last new interpretation combined with the algorithm we developed one can evaluate the SPR sensor sensitivity for different cases and structures. Sensitivity enhancement versus wavelength, prism refractive index, and the optimum dielectric layer thickness in the GWSPR configuration was examined. The correlation between the rigorous calculations of the sensitivity and the overlap integral was verified. The enhancement factor does not scale linearly with the wavelength as one might expect from the increase of the interaction volume, simply because the metal becomes more absorptive in the infrared region. Our theoretical study may help in the improvement and optimization of sensors based on SPR.

Appendix A.

Most of the optical sensing techniques are based on the existence of evanescent wave in the region where the analyte to be sensed is located. Examples are: TIR, ATR, SPR, fibers and waveguides, LSPR, micro-resonators, grating waveguide resonant structures, and resonant mirror sensors. Evanescent waves arise when there is a confinement region in which the majority of the optical density exists, however, outside this region a tail of the optical field exists forming the evanescent wave. Fig. A.1 shows a general schematic of the confinement region and the two bounding regions called substrate and cover or analyte.

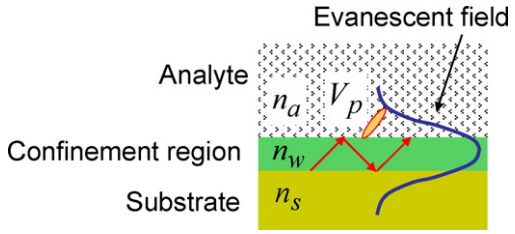

Fig. A.1. Schematic of the evanescent wave sensor based on planar optical waveguide.

The dielectric function of the structure can be written as [30]:

$$\varepsilon = \begin{cases} n_w^2 & r \in V_w \\ n_{a,s}^2 & r \notin V_w \end{cases} \tag{A.1}$$

where n_a, n_w, n_s are the refractive indices in the analyte, in the confinement (waveguide) region, and the substrate region, respectively, with V_w being the space volume of the confinement region. Assuming a particle with refractive index n_p is added to the analyte and caused a variation $\delta\varepsilon = n_a^2 - n_p^2$ in the dielectric function of the analyte within the volume of the particle V_p. The wave equation before the addition of the particle is:

$$\nabla \times \nabla \times E_i = k_i^2 \cdot \varepsilon \cdot E_i \tag{A.2}$$

where E_i, k_i are the electric field and the wave vector before the addition of the particle. After the addition of the particle, the electric field, the dielectric function and the wave vector changes to: E_f, $\varepsilon_f = \varepsilon + \delta\varepsilon$, $k_f = k_i + \delta k$, so that the wave equation becomes:

$$\nabla \times \nabla \times E_f = k_f^2 \cdot \varepsilon \cdot E_f \tag{A.3}$$

Multiplying by E_i^*, subtracting Eq. (A.2) from Eq. (A.3) and integrating over the entire volume leads to:

$$(k_i^2 - k_f^2) \int E_f \cdot \varepsilon \cdot E_i^* dr = k_f^2 \cdot \int_{V_p} E_i^* \cdot \delta\varepsilon \cdot E_f \cdot dr \tag{A.4}$$

Using first-order perturbation theory in k, we get:

$$\delta k \approx \frac{k_i}{2} \cdot \frac{\int_{V_p} \delta\varepsilon \cdot E_i^* \cdot E_f \cdot dr}{\int_V \varepsilon \cdot E_i^* \cdot E_i \cdot dr} \tag{A.5}$$

Hence the dielectric perturbation in the evanescence region caused a shift in the guided wave vector determined by the overlap integral normalized to the mode energy integral.

References

[1] I. Abdulhalim, M. Zourob, A. Lakhtakia, Surface plasmon resonance sensors: a mini review, Electromagnetics 28 (2008) 213–242.
[2] W.L. Barnes, A. Dereux, T.W. Ebbesen, Surface plasmon subwavelength optics, insight review article, Nature 424 (2003) 824–830.
[3] J.M. Pitarke, V.M. Silkin, E.V. chulkov, P.M. Echenique, Theory of surface plasmons and surface plasmons polaritons, Rep. Prog. Phys. 70 (2007) 1–87.
[4] H. Raether, Surface Plasmons on Smooth and Rough Surfaces and on Gratings, Springer Tracts in Modern Physics, Springer Verlag, 1988.
[5] E. Kretchmann, Decay of non radiative surface plasmons into light on rough silver films: comparison of experimental and theoretical results, Opt. Commun. 6 (1972) 185–187.
[6] A. Otto, Excitation of surface plasma waves in silver by the method of frustrated total reflection, Z. Phys. 216 (1968) 398–410.

[7] J.V. Gent, P.V. Lambeck, H.J.M. Kreuwel, G.J. Gerritsma, E.J.R. Sundholter, D.N. Beinhoudt, T.J. Popma, Optimization of chemooptical surface plasmon resonance based sensors, Appl. Opt. 29 (1990) 2843–2849.
[8] M. Golosovsky, V. Lirtsman, V. Yashunsky, D. Davidov, B. Aroeti, Mid infrared surface plasmon resonance: a novel biophysical tool for studying living cells, Appl. Opt. 105 (2009) 102036.
[9] R.T. Deck, D. Sarid, G.A. Olson, J.M. Elson, Coupling between finite electromagnetic beam and long-range surface plasmon mode, Appl. Opt. 22 (1983) 3397–3405.
[10] G.G. Nenningera, P. Tobislkab, J. Homola, S.S. Yee, Long-range surface plasmons for high-resolution surface plasmon resonance sensors, Sens. Actuators B: Chem. 74 (2001) 145–151.
[11] S. Pakkovsky, M. Meunier, A.V. Kabashin, Surface plasmon resonance polarizator for biosensing and imaging, Opt. Commun. 281 (2008) 5492–5496.
[12] J.Y. Lee, H.C. Shin, C.T. Hong, T.K. Chou, Measurement of refractive index change by surface plasmon resonance and phase quadrature inteferometry, Opt. Commun. 276 (2007) 283–287.
[13] S.F. Wang, M.H. Chiu, C.W. Lai, R.S. Chang, High-sensitivity small-angle sensor based on surface plasmon resonance technology and heterodyne interferometry, Appl. Opt. 45 (2006) 6702–6707.
[14] H.P. Ho, W. Yuan, C.L. Wong, S.Y. Wu, Y.K. Suen, S.K. Kong, C. Lin, Sensitivity enhancement based on application of multi-pass interferometry in phase-sensitive surface plasmon resonance biosensor, Opt. Commun. 275 (2007) 491–496.
[15] B. Ran, S.G. Lipson, Comparison between sensitivities of phase and intensity detection in surface plasmon resonance, Opt. Exp. 14 (2006) 5641–5650.
[16] C.J. Alleyne, A.G. Kirk, R.C. McPhedran, N.A.P. Nicorovici, D. Maystre, Enhanced SPR sensitivity using periodic metallic structures, Opt. Exp. 15 (2007) 8163–8169.
[17] W. Bin, W. Kang, High sensitivity transmission-type SPR sensor by using metallic-dielectric mixed gratings, Chem. Phys. Lett. 25 (2008) 1668–1671.
[18] S.A. Zynio, A.V. Samoylov, E.R. Surovtseva, V.M. Mirsky, Y.M. Shirshov, Bimetallic layers increase sensitivity of affinity sensors based on surface plasmon resonance, Sensors 2 (2002) 62–70.
[19] X.-C. Yuan, B.H. Ong, Y.G. Tan, D.W. Zhang, R. Irawan, S.C. Tjin, Sensitivity–stability-optimized surface plasmon resonance sensing with double metal layers, J. Opt. A: Pure Appl. Opt. 8 (2006) 959–963.
[20] B.H. Ong, X. Yuan, S.C. Tjuin, J. Zhang, H.M. Ng, Optimized film thickness for maximum field enhancement of a bimetallic surface plasmon resonance biosensor, Sens. Actuators B: Chem. 114 (2006) 1028–1034.
[21] G. Gupta, J. Kondoh, Tuning and sensitivity enhancement of surface plasmon resonance sensors, Sens. Actuators A 122 (2006) 381–388.
[22] J. Yulk, D. Hong, J. Jung, S. Jung, H. Kim, J. Han, Y. Kim, K. Ha, Sensitivity enhancement of spectral surface plasmon resonance biosensors for the analysis of protein arrays, Eur. Biophys. 35 (2006) 469–476.
[23] A. Lahav, M. Auslender, I. Abdulhalim, Sensitivity enhancement of guided wave surface plasmon resonance sensors, Opt. Lett. 33 (2008) 2539–2541.
[24] A. Lahav, A. Shalabney, I. Abdulhalim, Surface plasmon resonance sensor with enhanced sensitivity using nano-top dielectric layer, J. Nanophoton. 3 (2009) 031501.
[25] Z. Salamon, H.A. Macleod, G. Tollin, Surface plasmon resonance spectroscopy as a tool for investigating the biochemical and biophysical properties of membrane protein system. I. Theoretical principles, Biochim. Biophys. Acta 1331 (1997) 117–129.
[26] Z. Salamon, H.A. Macleod, G. Tollin, Surface plasmon resonance spectroscopy as a tool for investigating the biochemical and biophysical properties of membrane protein system. II. Applications to biological systems, Biochim. Biophys. Acta 1331 (1997) 131–152.
[27] S. Toyama, N. Doumae, A. Shoji, Y. Ikariyama, Design and fabrication of a waveguide-coupled prism device for surface plasmon resonance sensor, Sens. Actuators B 65 (2000) 32–34.
[28] Z. Salamon, G. Tollin, Optical anisotropy in lipid bilayer membranes: coupled plasmon-waveguide resonance measurements of molecular orientation, polarizability, and shape, Biophys. J. 80 (2001) 1557–1567.
[29] J.M. McDonnell, Surface plasmon resonance: towards an understanding of the mechanisms of biological molecular recognition, Curr. Opin. Chem. Biol. 5 (2001) 572–577.
[30] I. Abdulhalim, Biosensing configurations using guided wave resonant structures, in: W.J. Bock, I. Gannot, S. Tanev (Eds.), NATO Science for Peace and Security Series B: Physic sand Biophysics, Optical Waveguide Sensing and Imaging, Springer-Verlag, Netherlands, 2007, pp. 211–228, doi:10.1007/978-1-4020-6952-9_9.
[31] T.J. Davis, Surface plasmon modes in multi-layer thin-films, Opt. Commun. 282 (2009) 135–140.
[32] C.B. Su, J. Kameoka, Forty four pass fiber-optic loop for improving the sensitivity of surface plasmon resonance sensors, Meas. Sci. Technol. 19 (2008), 015204 (5 pp.).
[33] K. Ohta, H. Ishida, Matrix formalism for calculation of electric field intensity of light in stratified multilayered films, Appl. Opt. 29 (1990) 1952–1959.
[34] S. Ekgasit, C. Thammacharoen, W. Knoll, Surface plasmon resonance spectroscopy based on evanescent field treatment, Anal. Chim. 76 (2004) 561–568.
[35] W. Hansen, Electric fields produced by the propagation of plane coherent electromagnetic radiation in a stratified medium, Opt. Soc. Am. 58 (1968) 380–390.
[36] M. Born, E. Wolf, Principles of Optics, Electromagnetic Theory of propagation, Interface and Diffraction of Light, 5th ed., Pergamon Press, 1975, pp. 56–62.
[37] J. Homola, I. Koudela, S.S. Yee, Surface plasmon resonance sensors based on diffraction gratings and prism couplers: sensitivity comparison, Sens. Actuators A 54 (1999) 16–24.

Biographies

Atef Shalabney was born in August 30, 1973 in Iksal village in Israel. Received his bachelor of sciences in electrical engineering from the Technion, Institute of Technology, Hafia, Israel in 1997, and a master degree in electro-optics engineering from the Ben Gurion University, Beer Shiva, Israel in 2009. Currently, he is a PhD student in electro-optics engineering at Ben Gurion University. His research interests are plasmonic structures and optical biosensing devices.

Prof. Ibrahim Abdulhalim was born in Kafr Manda, Israel in November 22, 1957. He studied Physics at the Technion, Haifa, where he received his BSc, MSc and DSc in 1982, 1985 and 1988, respectively. He spent several years working in applied optics in academia and industry such as in the University of Colorado at Boulder, in the ORC at Southampton University, in the University of Western Scoltalnd, in KLA-Tencor Corporation, in Nova Measuring Instruments and in GWS-Photonics. In October 2005 he joined the Ben Gurion University, department of electro-optic engineering as an associate professor. His current research activities involve nanophotonic structures for biosensing, improved biomedical optical imaging techniques such as spectropolarimetric imaging and full field optical coherence tomography. Prof. Abdulhalim has published over 80 journal articles, 50 conference proceedings papers, and 10 patents. He became a fellow of the Institute of Physics, UK in 2004. He is an associate editor of the SPIE Journal of NanoPhotonics for the fourth year now.